Article:
Partridge, B.E., Leowanawat, P., Aqad, E. et al. (2015) Increasing 3D Supramolecular Order by Decreasing Molecular Order. A Comparative Study of Helical Assemblies of Dendronized Nonchlorinated and Tetrachlorinated Perylene Bisimides. Journal of the American Chemical Society, 137 (15). pp. 5210-5224. ISSN: 0002-7863

https://doi.org/10.1021/jacs.5b02147

Increasing 3D Supramolecular Order by Decreasing Molecular Order. A Comparative Study of Helical Assemblies of Dendronized Non-Chlorinated and Tetrachlorinated Perylene Bisimides

Benjamin E. Partridge,[†] Pawaret Leowanawat,[†] Emad Aqad,[†] Mohammad R. Imam,[†] Hao-Jan Sun,[†, ‡] Mihai Peterca,[†] Paul A. Heiney,[‡] Robert Graf,[§] Hans W. Spiess,[§] Xiangbing Zeng,[¶] Goran Ungar,[¶,#] Virgil Percec*[,†]

[†]Roy & Diana Vagelos Laboratories, Department of Chemistry, University of Pennsylvania, Philadelphia, Pennsylvania 19104-6323, United States. [‡]Department of Physics and Astronomy, University of Pennsylvania, Philadelphia, Pennsylvania 19104-6396, United States. [§]Max-Planck Institute for Polymer Research, 55128 Mainz, Germany. [¶]Department of Materials Science and Engineering, University of Sheffield, Sheffield S1 3JD, United Kingdom. [#]Department of Applied Chemistry, National Chiao Tung University, Hsin-Chu 30049, Taiwan.

*E-mail: percec@sas.upenn.edu

ABSTRACT: A non-planar, twisted tetrachlorinated perylene bisimide (Cl_4PBI) was functionalized with two AB_3 minidendrons containing either hydrogenated or semifluorinated dodecyl groups. The hydrogenated dendron was attached to the imide groups of Cl_4PBI via zero, one and two (m = 0, 1 and 2) methylenic units, whereas the dendron containing semifluorinated groups was attached via m = 3 or a di(ethylene oxide) linker (m = 2EO). The supramolecular structures of these compounds determined by a combination of differential scanning calorimetry, X-ray diffraction and solid state NMR, were compared with those of non-chlorinated PBI reported previously, which demonstrated the thermodynamically controlled formation of 2D periodic arrays at high temperatures and 3D arrays at low temperatures. The molecularly less ordered Cl_4PBI containing hydrogenated dendrons self-organize into exclusively 3D crystalline periodic arrays under thermodynamic control for m = 0 and 2 while the more highly molecularly ordered PBI produced less stable and ordered 3D crystals and also 2D assemblies. *This induction of a higher degree of 3D order in supramolecular assemblies of the less well-ordered molecular building blocks was unanticipated.* The semifluorinated dendronized Cl_4PBI with m = 3 formed a 2D columnar hexagonal array under kinetic control, whereas the compound with m = 2EO formed an unusual 2D honeycomb-like hexagonal phase under thermodynamic control. These Cl_4PBI compounds provide a new route to stable crystalline assemblies via thermodynamic control at lower temperatures than previously obtained with PBI, thus generating 3D order in an accessible range of temperature of interest for structural analysis and for technological applications.

INTRODUCTION

Supramolecular assemblies of perylene bisimides (PBI) have been extensively studied for a wide range of functions, such as industrial pigments,[1] as mimics of biological systems[2–4] and as *n*-type semiconductors for organic electronics including solar cells.[5,6] Practical applications of these systems are hampered by many issues, including poor solubility, high melting temperatures, air sensitivity, difficult processability, low charge carrier mobilities and short charge carrier lifetimes.[1,5,7,8] Furthermore, the kinetically controlled polymorphism of large PBI assemblies hinders their structural analysis,[9–11] especially by commonly-used single crystal X-ray diffraction analysis. Functionalization of the *bay* positions of PBI with halogens including fluorine, chlorine and bromine has been proven to address some of the limitations of non-halogenated PBI building blocks.[5] In particular, halogenation increases the electron acceptor ability of PBI and extends the lifetime of charge carriers.[1,7,12] Indeed, the electronic properties of non-halogenated PBIs and halogenated PBIs have been compared in many laboratories.[5,6,12–14] However, detailed comparative studies of the complex supramolecular structures formed by the self-assembly of planar non-chlorinated PBIs and non-planar tetrachlorinated PBI (Cl_4PBI) are not available.

Our laboratory has previously reported a series of non-halogenated PBI derivatives functionalized at the imide positions with two first generation self-assembling minidendrons, (3,4,5)*n*G1-*m*-PBI (where *n* is the number of carbons in the alkyl groups and *m* is the number of methylenic units between the dendron and the imide group of PBI).[9–11] The PBI derivatives self-organized to form a range of 2D and 3D phases, of which the 3D thermodynamic products are the most desirable for technological applications.[11] Here we report the synthesis and structural analysis of five Cl_4PBI derivatives with *n* and *m* chosen to promote thermodynamically controlled formation of 3D crystalline phases.[9–11] Cl_4PBI compounds were synthesized with *m* = 0, 1, 2, 3 and 2EO (where EO is ethylene oxide, $–CH_2CH_2O–$), functionalized at their imide groups with first generation self-assembling dendrons with either dodecyl groups (**8a**, **8b** and **8c** with *m* = 0, 1 and 2, respectively) or semifluorinated groups, $–CH_4(CF_2)_7CF_3$ (denoted 12F8; **9** and **11** with *m* = 3 and 2EO, respectively), at the periphery of the dendrons. A detailed structural study of the

assemblies formed by these Cl_4PBI derivatives is described and compared with the self-assembling behavior of non-chlorinated PBI derivatives. Knowledge of the precise influence of tetrachlorination on the structural properties of PBI derivatives at the molecular level, as elucidated here, will find widespread utility in the future design of complex supramolecular materials for a variety of applications.

RESULTS AND DISCUSSION

Synthesis of Dendronized PBI and Semifluorinated Dendronized Cl_4PBI. The synthesis of the semifluorinated dendronized amine **6** is outlined in Scheme 1. The synthesis of hydrogenated dendronized tetrachlorinated PBIs (3,4,5)12G1-*m*-Cl_4PBI with m = 1, 2 and 3 (**8a–c**) and semifluorinated dendronized tetrachlorinated PBIs (3,4,5)12F8G1-3-Cl_4PBI (**9**) and (3,4,5)12F8G1-2EO-Cl_4PBI (**11**) is outlined in Scheme 2.

Scheme 1. Synthesis of Semifluorinated Dendronized Amine **6**

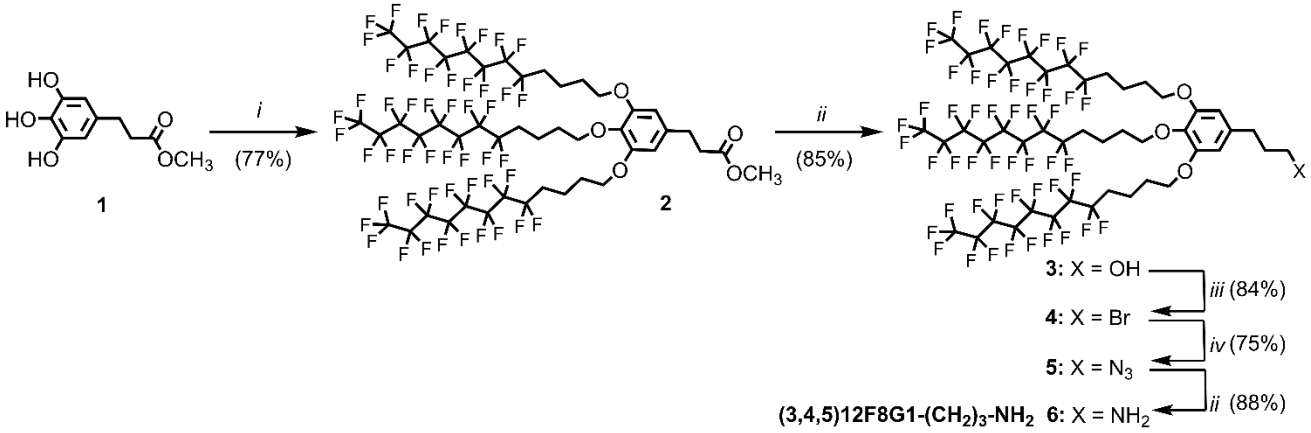

Reagents and conditions: (i) $C_8F_{17}(CH_2)_4Br$, K_2CO_3, DMF (75 °C); (ii) $LiAlH_4$, THF (0–25 °C); (iii) CBr_4, PPh_3, CH_2Cl_2 (25 °C); (iv) NaN_3, DMF (85 °C)

Methyl 3-(3,4,5-trihydroxyphenyl)propanoate **1** was synthesized according to a procedure previously reported by our laboratory.[15] Minidendron **2** was prepared in 77% yield via the etherification of 1H,1H,2H,2H,3H,3H,4H,4H-perfluorododecyl bromide that was synthesized as reported previously[16] with **1** in dry DMF with potassium carbonate as base. The dendritic carboxylic ester **2** was reduced with $LiAlH_4$ in dry THF to afford alcohol **3** in 85% yield. Preparation of amine **6** proceeded via bromination of **3** with carbon tetrabromide and PPh_3 in dry CH_2Cl_2 to give bromide **4** in 84% yield, followed by treatment with sodium azide in dry DMF to give azide **5** in 75% yield.[15] Subsequent reduction of azide **5** by $LiAlH_4$ in dry THF afforded the semifluorinated dendritic amine **6** in 88% yield.

Scheme 2. Synthesis of Hydrogenated Dendronized Cl_4PBIs **8a**, **8b** and **8c** (*m* = 1, 2 and 3) and Semifluorinated Dendronized Cl_4PBIs **9** (*m* = 3) and **11** (*m* = 2EO)

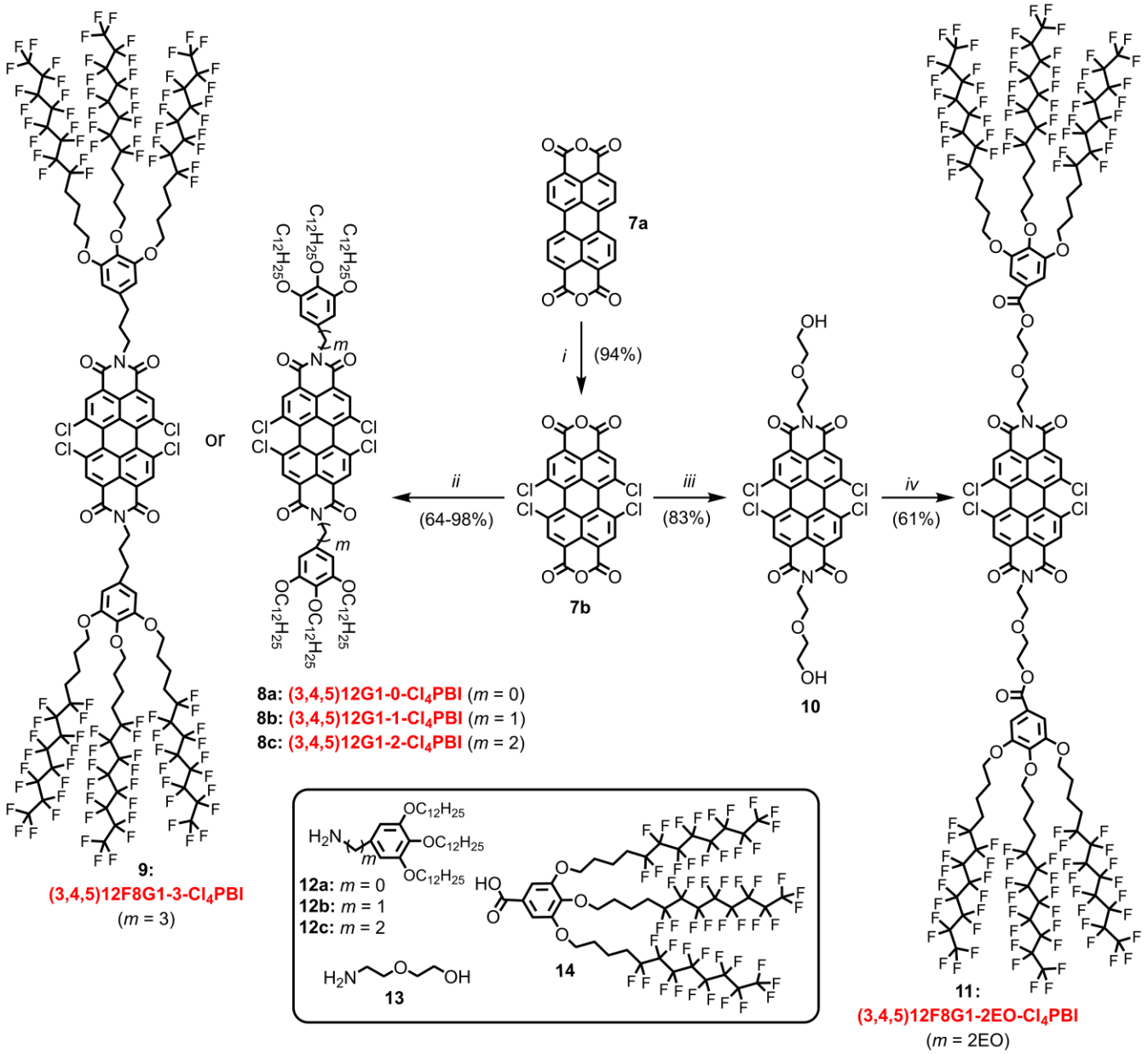

Reagents and conditions: (i) I_2, chlorosulfonic acid (65 °C); (ii) **12a**, **b**, **c** or **6**, $Zn(OAc)_2{\cdot}2H_2O$, quinoline (180 °C); (iii) **13**, $Zn(OAc)_2{\cdot}2H_2O$, pyridine (120 °C); (iv) **14**, PPh_3, DIAD, THF (25 °C)

Tetrachlorination of perylene-3,4,9,10-tetracarboxylic dianhydride was achieved using a modified literature procedure.[17] Treatment of perylene-3,4,9,10-tetracarboxylic dianhydride (**7a**) with chlorosulfonic acid and a catalytic amount of iodine for 20 h at 65 °C afforded tetrachlorinated **7b** in 94% yield. The hot reaction mixture was filtered to remove the insoluble unreacted starting material and insoluble by-products to afford pure **7b**. In contrast to poorly soluble red starting material **7a,** tetrachlorinated **7b** is orange and shows moderate solubility in both THF and chloroform.

PBI derivatives **8a**, **8b** and **8c** were prepared by imidation of **7b** in one step. Dianhydride **7b** was treated with dendritic amines **12a**, **12b** and **12c**, all previously reported from our laboratory,[9] and zinc acetate dihydrate in quinoline at 180 °C.[10] Purification by column chromatography on silica gel using CH_2Cl_2 as eluent, followed by precipitation in MeOH, afforded hydrogenated dendronized tetrachlorinated PBI derivatives **8a**, **8b** and **8c** in 69%, 84% and 98% yields, respectively. The same procedure was employed to synthesize semifluorinated compound **9** in 64% yield from dianhydride **7b** and semifluorinated dendritic amine **6**.

Preparation of semifluorinated compound **11** with a di(ethylene oxide) linker was achieved in two steps from dianhydride **7b**. The ethylene oxide motif was first installed by treatment of **7b** with commercially available 2-(2-aminoethoxy)ethanol (**13**) and zinc acetate dihydrate in pyridine at 120 °C. Anhydride **10**, thus obtained in 83% yield, was then coupled with dendritic carboxylic acid **14**, previously reported from our laboratory[16], via a Mitsunobu reaction. Treatment of **10** with **14**, diisopropyl diazocarboxylate (DIAD) and PPh_3 in dry THF, followed by purification by column chromatography (silica gel, CH_2Cl_2 as eluent) and precipitation into MeOH afforded semifluorinated dendronized tetrachlorinated PBI derivative **11** in 61% yield.

Figure 1 shows the ^{1}H NMR spectra for the five Cl_4PBI derivatives **8a–c**, **9** and **11**, which exhibit signals pertaining to the protons of the perylene core (*a*), the aromatic protons of the dendron (*b*) and the protons of the –OC*H*$_2$– units in the dendritic alkyl groups (*c*). The chemical shift of the perylene-based aromatic protons (*a*) is very similar in all five compounds, indicating the minimal electronic interaction between the PBI core and imide substituents, due primarily to a nodal plane in the LUMO and HOMO of substituted PBIs.[5] Also notable is the downfield shift (~0.4 ppm) of the signal from the aromatic protons of the dendron (*b*) in compound **8b** due to enhanced deshielding by the adjacent methylene unit.

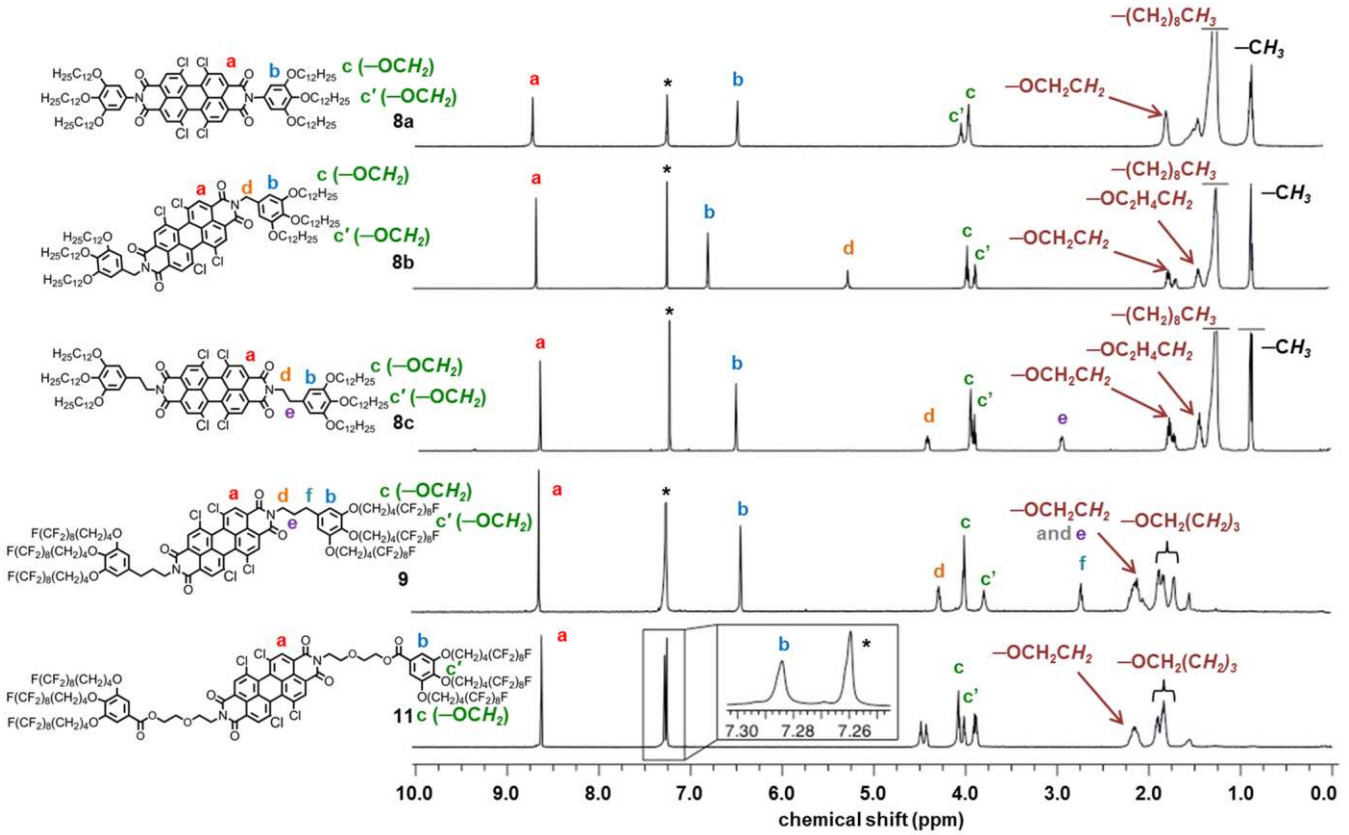

Figure 1. ^{1}H NMR spectra ($CDCl_3$, 500 MHz, 298 K) of hydrogenated dendronized tetrachlorinated PBIs **8a**, **8b** and **8c** (m = 0, 1 and 2) and semifluorinated dendronized tetrachlorinated PBIs **9** (m = 3) and **11** (m = 2EO). Residual solvent peak ($CHCl_3$) is denoted by an asterisk.

Motivation for Incorporation of Semifluorinated Dendrons. Extensive studies from our laboratory have demonstrated that semifluorination of first[16,18] and higher[19,20] generation self-assembling dendrons increases the thermal stability of their supramolecular assemblies without affecting their supramolecular structure, with one exception,[21] even with very bulky[22–25] apical substituents. In self-assembling dendrons with peripheral *n*-dodecyl substituents, it has been demonstrated that substitution of eight out of the twelve methylenic units with perfluorinated CF_2 segments[16] provides an optimum degree of semifluorination that enhances the thermal stability of various supramolecular assemblies. These results were explained by the higher stiffness of linear perfluoroalkanes compared to perhydrogenated alkanes. However, nonlinear semifluorinated compounds can exhibit lower stability than analogous hydrogenated compounds.[26,27] DSC data to be discussed later show that the thermal stability of Cl_4PBIs **8a–c** decreases with increasing linker length, and that the melting temperature of m = 2 compound **8c** was already below that of interest for this study. Therefore, semifluorinated dendrons were incorporated into m = 3 Cl_4PBI

compound, **9**. For an even larger value of *m*, di(ethylene oxide), shown previously to promote formation of crystalline phases,[23] was chosen to replace the methylenic groups, affording the semifluorinated Cl_4PBI derivative **11** (*m* = 2EO).

Structural Analysis of Supramolecular Assemblies of Cl_4PBI Dendronized with Hydrogenated Dendrons by Differential Scanning Calorimetry (DSC) and X-ray Diffraction (XRD). It was previously reported that non-chlorinated PBIs form crystalline phases via a kinetically controlled process which is highly dependent on thermal treatment (i.e., rates of heating and cooling, and periods of annealing). Thermodynamically controlled formation of 3D crystalline phases was first discovered in our laboratory for a range of non-chlorinated dendronized PBI derivatives.[9–11] Whether an ordered periodic array is self-organized via a thermodynamically or kinetically controlled process can be assessed by analysis of DSC experiments performed at different rates. Thermodynamically controlled phase transitions show no scan rate dependence and little supercooling, whereas transitions occurring via a kinetically controlled process show a significant dependence on the scan rate and may show significant supercooling. Figure 2 shows the DSC traces of first heating (left), first cooling (middle), and second heating cycles (right) obtained with scan rates of 10 °C/min and 1 ºC/min for the hydrogenated dendronized Cl_4PBIs **8a–c**. The phases denoted in Figure 2 were identified via X-ray diffraction (XRD) experiments to be discussed later.

In contrast to previously reported PBIs,[9] which self-organize in 2D periodic arrays and 2D assemblies with intracolumnar order, the current Cl_4PBIs **8a–c** form only 3D crystalline phases below the isotropization temperature, T_i (Figure 2). This suggests that the Ti of the Cl_4PBIs is reduced by a sufficient extent as to bypass the temperature range in which 2D phases would be formed. This also demonstrates the ability to develop intercolumnar correlations even at high temperature, despite the lack of planarity in the PBI unit that results from chlorination of the core.[7,13] However, the T_i of the Cl_4PBIs **8a–c** is significantly lower than the T_i of the non-chlorinated analogs, with a maximum difference of 149 °C for **8a**. In previous studies, the full phase behavior of the non-chlorinated *m* = 0 compound could not be investigated by XRD due to its exceedingly high value of T_i (361 °C), that lies outside the

temperature range of our X-ray instrumentation. Tetrachlorination of the m = 0 compound lowers T_i to 212 °C, and therefore the entire temperature range occupied by the assemblies of **8a** is accessible for analysis by XRD (to be discussed later). Thus, tetrachlorination facilitates the investigation of high temperature assemblies in structurally-related non-chlorinated PBI derivatives whose supramolecular assemblies occur at otherwise inaccessibly high temperatures. The decrease in T_i exhibited by assemblies of **8a–c** as compared to non-chlorinated analogs indicates that chlorination of the PBI core destabilizes the thermal stability of the assemblies of PBI.

The elongation of the linker between dendron and PBI core also has notably different impacts on T_i for PBI and Cl_4PBI. The disparity in T_i between PBI and Cl_4PBI compounds becomes less marked as the number of methylene units between the dendron and PBI core increases. Whereas T_i of m = 0 Cl_4PBI compound **8a** is 149 °C lower than that of the m = 0 PBI, this difference decreases to 119 °C for m = 1 and only 24 °C for m = 2. Furthermore, elongation of the linker by one methylene unit from m = 1 to m = 2 in Cl_4PBIs **8b** and **8c** has negligible impact on T_i. Conversely, the non-chlorinated PBI with m = 1 has a T_i that is 91 °C higher than the non-chlorinated PBI with m = 2. This smaller influence of linker length in the tetrachlorinated systems indicates that the spatial arrangement of the PBI core plays a more significant role in the thermal behavior of Cl_4PBI assemblies than in the behavior of non-chlorinated PBIs. A significant contribution to the spatial arrangement of the Cl_4PBI derivatives is the twisting of the PBI core caused by steric and electronic repulsions between the chlorine atoms at the *bay* positions. Previous single crystal XRD studies have shown that the Cl_4PBI core is twisted by 35–37° in tetrachlorinated PBI derivatives, and that the degree of twisting is mostly invariant with respect to the identity of the groups attached at the imide positions.[7,13] This is in contrast to the planarity of the PBI core in non-chlorinated PBI molecules.

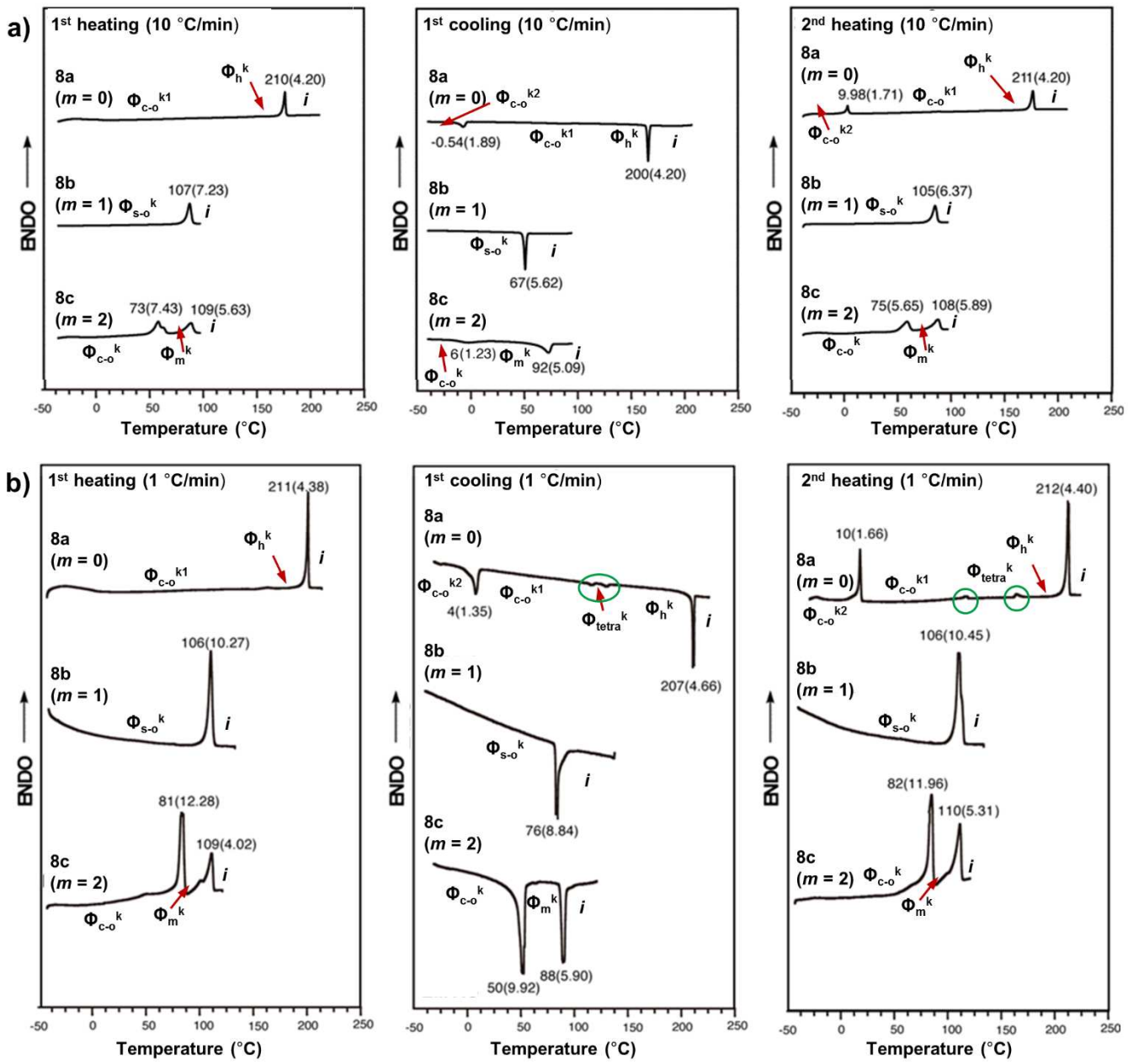

Figure 2. DSC traces of hydrogenated dendronized Cl_4PBIs **8a**, **8b** and **8c** (*m* = 1, 2 and 3) recorded with heating and cooling rates of (a) 10 °C/min and (b) 1 °C/min. Phases determined by XRD, transition temperatures, and associated enthalpy changes (in parentheses in kcal/mol) are indicated.

Four crystalline periodic arrays were identified for the Cl_4PBI *m* = 0 compound **8a** (Figure 2). Three of these arrays ($\mathbf{\Phi_{c\text{-}o}^{k1}}$, $\mathbf{\Phi_{c\text{-}o}^{k2}}$ and $\mathbf{\Phi_h^k}$) are formed via thermodynamically controlled transitions, as indicated by their invariant transition temperatures at differing scan rates (compare Figure 2a with Figure 2b). A fourth phase, the tetragonal $\mathbf{\Phi_{tetra}^k}$ phase, is observed only by scanning at a rate of 1 ºC/min (Figure 2b), and is therefore kinetically controlled. The two orthorhombic crystalline phases of **8a** ($\mathbf{\Phi_{c\text{-}o}^{k1}}$ and $\mathbf{\Phi_{c\text{-}o}^{k2}}$) have similar supramolecular column arrangements, and their structural difference

most likely lies in the crystallization of the alkyl matrix at low temperature. Interestingly, a hexagonal crystal phase ($\mathbf{\Phi_h^k}$) was observed at high temperature. The lattice symmetry of $\mathbf{\Phi_h^k}$ requires that the unit cell contains only one single column. This implies that the supramolecular columns within a single crystal domain should possess identical handedness and are therefore homochiral within that crystal domain. This further implies that the crystal phase is likely a supramolecular conglomerate containing pure right-handed and left-handed domains.[28] The formation of four phases, three of which are formed under thermodynamic control, contrasts with the formation of only a single low order crystalline phase via a slow, kinetically controlled process in the non-chlorinated m = 0 compound. Therefore, chlorination of the PBI core transforms the crystallization of the m = 0 system from kinetic to thermodynamic control. A similar molecule reported by the Würthner laboratory featuring dodecyl ($CH_3(CH_2)_{11}$–) groups rather than dodecyloxy ($CH_3(CH_2)_{11}O$–) groups in the dendron, also exhibits multiple crystalline phases during the first heating scan by DSC.[7] However, none of these phases are thermodynamically controlled. In addition, T_i for the Würthner laboratory's compound is 110 °C, over 100 °C lower than **8a** (T_i = 211 °C). This comparison indicates that the minidendrons containing alkoxy groups, with an ether oxygen, stabilize the supramolecular assembly more than the minidendrons containing alkyl groups, without an ether oxygen.

Only one crystal phase ($\mathbf{\Phi_{s\text{-}o}^k}$) is exhibited by the Cl_4PBI m = 1 compound **8b**. This phase, formed via a kinetically controlled process, is similar in its molecular and supramolecular arrangement to the single phase exhibited by the non-chlorinated m = 1 compound (Figure 4). However, the $\mathbf{\Phi_{s\text{-}o}^k}$ phase of the Cl_4PBI can be generated during cooling at a rate of 10 °C/min (Figure 2a), whereas formation of the crystalline phase in the non-chlorinated PBI analog requires slower cooling (1 °C/min) and annealing at room temperature for 3 h. Furthermore, the melting temperature of the crystalline phase of the Cl_4PBI (106 °C) is significantly higher than that of the non-chlorinated compound (36 °C). These data highlight the unexpected ability of the Cl_4PBI core to enhance crystalline order through molecular disorder in the m = 1 system.

Cl_4PBI and PBI with m = 2 exhibit a low temperature orthorhombic crystal phase formed under kinetic control. This phase is obtained with a cooling rate of 10 °C/min (Figure 2a) in the Cl_4PBI m = 2 compound, but could only be developed in a narrow range of temperature (91–101 °C) with slow heating (1 °C/min) in the corresponding non-chlorinated PBI. The m = 2 Cl_4PBI **8c** also has a thermodynamically controlled 3D monoclinic crystalline phase at higher temperature. No such phase is exhibited by the non-chlorinated PBI.

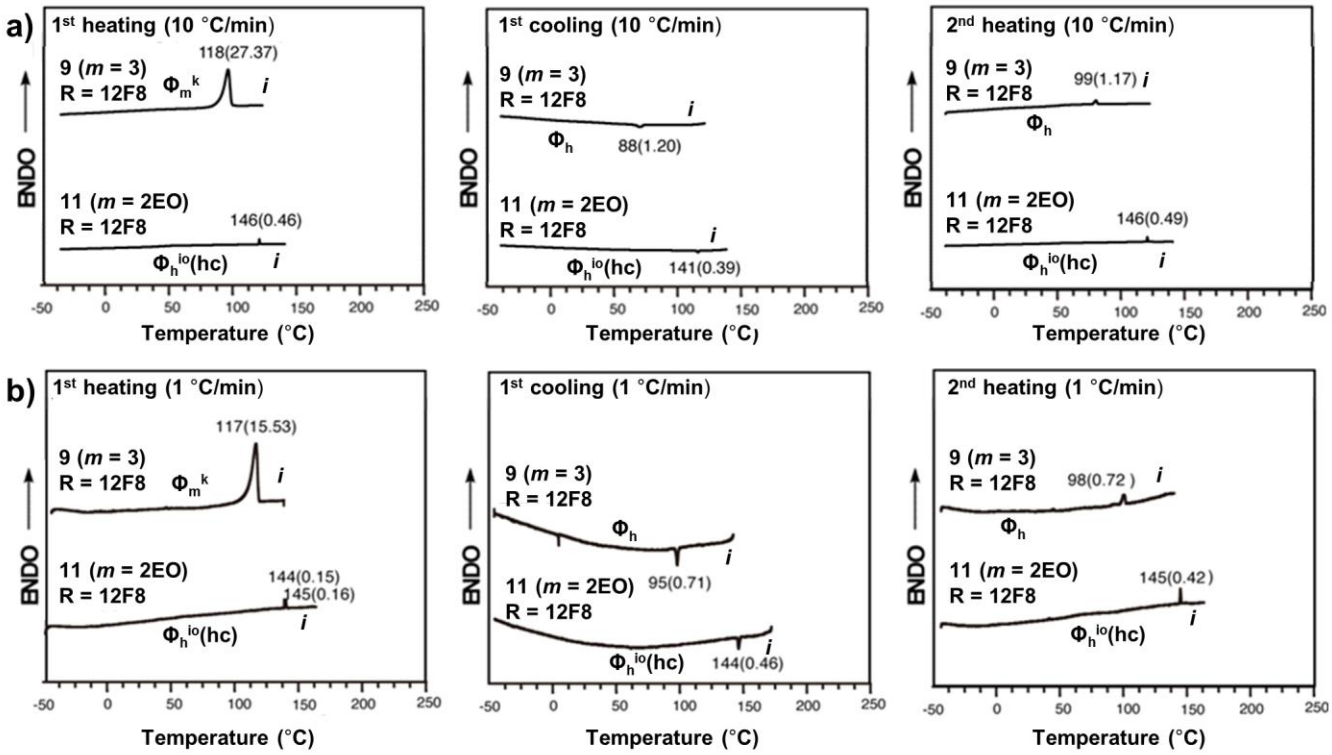

Figure 3. DSC traces of semifluorinated dendronized tetrachlorinated PBIs **9** (m = 3) and **11** (m = 2EO) recorded with heating and cooling rates of (a) 10 °C/min and (b) 1 °C/min. Phases determined by XRD, transition temperatures, and associated enthalpy changes (in parentheses in kcal/mol) are indicated.

All three hydrogenated dendronized Cl_4PBIs exhibit crystalline phases during cooling at a rate of 10 °C/min (Figure 2a). Thermodynamically controlled crystallization was observed in the m = 0 and m = 2 compounds. In contrast, all crystalline phases in the non-chlorinated counterparts are kinetically controlled and none of them can be detected by DSC with a cooling rate of 10 °C/min or faster. Therefore, unpredictably, chlorination of the bay position of the PBI core transforms the PBI into a non-planar twisted molecule that stabilizes 3D crystalline phases and encourages their formation under thermodynamic control.

Table 1. Thermal Analysis of Hydrogenated Dendronized Cl_4PBIs **8a**, **8b** and **8c** (*m* = 1, 2 and 3) and Semifluorinated Dendronized Cl_4PBIs **9** (*m* = 3) and **11** (*m* = 2EO)

		Phases, transition temperatures (°C) and corresponding enthalpy changes (in parentheses, kcal/mol)	
Compound	Rate (ºC/min)	Heating[a]	Cooling
8a (*m* = 0)	10	$\Phi_{c\text{-}o}^{k1}$ –[b] Φ_h^k 210 (4.20) ***i***	***i*** 200 (–4.20) Φ_h^k –[b] $\Phi_{c\text{-}o}^{k1}$ –0.5 (–1.89) $\Phi_{c\text{-}o}^{k2}$
		$\Phi_{c\text{-}o}^{k2}$ 10 (1.71) $\Phi_{c\text{-}o}^{k1}$ –[b] Φ_h^k 211 (4.20) ***i***	
	1	$\Phi_{c\text{-}o}^{k1}$ –[b] Φ_h^k 211 (4.38) ***i***	***i*** 207 (–4.66) Φ_h^k –[b] Φ_{tetra}^k –[b] $\Phi_{c\text{-}o}^{k1}$ 4 (–1.35) $\Phi_{c\text{-}o}^{k2}$
		$\Phi_{c\text{-}o}^{k2}$ 10 (1.66) $\Phi_{c\text{-}o}^{k1}$ –[b] Φ_{tetra}^k –[b] Φ_h^k 212 (4.40) ***i***	
8b (*m* = 1)	10	$\Phi_{s\text{-}o}^k$ 107 (7.23) ***i***	***i*** 67 (–5.62) $\Phi_{s\text{-}o}^k$
		$\Phi_{s\text{-}o}^k$ 105 (6.37) ***i***	
	1	$\Phi_{s\text{-}o}^k$ 106 (10.27) ***i***	***i*** 76 (–8.84) $\Phi_{s\text{-}o}^k$
		$\Phi_{s\text{-}o}^k$ 106 (10.45) ***i***	
8c (*m* = 2)	10	$\Phi_{c\text{-}o}^k$ 73 (7.43) Φ_m^k 109 (5.63) ***i***	***i*** 92 (–5.09) Φ_m^k –[b] $\Phi_{c\text{-}o}^k$
		$\Phi_{c\text{-}o}^k$ 75 (5.65) Φ_m^k 108 (5.89) ***i***	
	1	$\Phi_{c\text{-}o}^k$ 81 (12.28) Φ_m^k 109 (4.02) ***i***	***i*** 88 (–5.90) Φ_m^k 50 (–9.92) $\Phi_{c\text{-}o}^k$
		$\Phi_{c\text{-}o}^k$ 82 (11.96) Φ_m^k 110 (5.31) ***i***	
9 (*m* = 3)	10	Φ_m^k 118 (27.37) ***i***	***i*** 88 (–1.20) Φ_h
		Φ_h 99 (1.17) ***i***	
	1	Φ_m^k 117 (15.53) ***i***	***i*** 95 (–0.71) Φ_h
		Φ_h 98 (0.72) ***i***	
11 (*m* = 2EO)	10	Φ_h^{io}**(hc)** 146 (0.46) ***i***	***i*** 141 (–0.39) Φ_h^{io}**(hc)** –[b] Φ_h^{io}**(hc)**
		Φ_h^{io}**(hc)** 146 (0.49) ***i***	
	1	Φ_h^{io}**(hc)** 145 (0.16) ***i***	***i*** 144 (–0.46) Φ_h^{io}**(hc)** –[b] Φ_h^{io}**(hc)**
		Φ_h^{io}**(hc)** 145 (0.42) ***i***	

[a] Data from the first heating and cooling scans are on the first line, and data from the second heating are on the second line; $\Phi_{c\text{-}o}^k$ – columnar crystalline centered orthorhombic phase; Φ_h^k – columnar crystalline hexagonal phase; Φ_{tetra}^k – columnar crystalline tetragonal phase; $\Phi_{s\text{-}o}^k$ – columnar crystalline simple orthorhombic phase; Φ_m^k – columnar monoclinic crystalline phase; Φ_h – 2D columnar hexagonal phase; Φ_h^{io}**(hc)** – honeycomb-like 2D hexagonal phase with intracolumnar order; ***i*** – isotropic state; [b] This transition is observed by XRD. Note: quantitative uncertainties are ±1 ºC for thermal transition temperatures and ~2% for the associated enthalpy changes reported in kcal/mol.

Structural Analysis of Supramolecular Assemblies of Cl_4PBI Dendronized with Semifluorinated Dendrons by DSC and XRD. DSC traces of first heating (left), first cooling (middle), and second heating cycles (right) obtained with scan rates of 10 °C/min and 1 ºC/min for the semifluorinated dendronized PBIs **9** (*m* = 3) and **11** (*m* = 2EO) are shown in Figure 3. Neither compound exhibited a persistent 3D crystalline phase by DSC at scan rates of 10 °C/min (Figure 3a) and 1 °C/min (Figure 3b). The longer spacer length between the dendron and PBI core, and the presence of semifluorinated alkyl chains, completely suppresses intercolumnar correlations. The supramolecular columns assembled from *m* = 3 compound **9** generate a 2D hexagonal Φ_h array under thermodynamic control, similar to the non-chlorinated hydrogenated *m* = 3 counterpart. However, the 2D Φ_h phase is the only phase exhibited by **9**, showing that tetrachlorination of the PBI core eliminates completely the kinetically controlled formation of the $\Phi_{s\text{-}o}^k$ phase observed in the non-chlorinated hydrogenated *m* = 3 compound. The compound with *m* = 2EO (**11**) self-assembled into an uncommon honeycomb-like 2D hexagonal structure (Φ_h^{io}**(hc)**). The Φ_h^{io}**(hc)** phase is the only phase exhibited by **11** and is formed under thermodynamic control. Unlike other columnar phases, in which the center of each column consists of

stacked PBI cores, the columns of the Φ_h^{io}**(hc)** phase contain aggregated semifluorinated alkyl chains at their center (to be discussed in more detail later). The phase behavior and transition temperatures of **8a–c**, **9** and **11** as determined by DSC and XRD, are summarized in Table 1.

Structural Analysis of Cl_4PBIs Dendronized with Hydrogenated Dendrons by Small- (SAXS) and Wide-Angle X-ray Scattering (WAXS). The self-assembled structures of the dendronized Cl_4PBIs reported in Figure 2 and Figure 3 were determined by the analysis of their SAXS and WAXS patterns recorded as a function of temperature. Heating and cooling rates of 10 °C/min and 1 °C/min were employed in order to reproduce the experimental conditions applied in the DSC measurements.

Figure 4 shows the SAXS (Figure 4a–d) and WAXS (Figure 4e–h) patterns together with the corresponding indexing of the reflections and lattice parameters of the 3D periodic arrays assembled from $m = 0$ Cl_4PBI compound **8a**. Combined with the measured density at room temperature (1.09 g/cm^3) and the lattice volume, it was determined that the supramolecular columns in all observed crystal structures are constructed with only one dendronized PBI molecule in each column stratum. In the low temperature $\Phi_{c\text{-}o}^{k1}$ and $\Phi_{c\text{-}o}^{k2}$ phases, there are two columns in the unit cell, while in the high temperature Φ_{tetra}^{k} and Φ_h^k phases there is only one column in the unit cell, implying that helical columns in a single crystal domain are homochiral.[28] Although the small angle diffraction patterns differ substantially between phases, indicating different intercolumnar arrangements, the high similarity of the wide angle patterns (Figure 4e–h) suggests that the intracolumnar order and π–π stacking distance are similar for all phases exhibited by **8a**. In the wide angle patterns, a strong meridional reflection with a *d*-spacing of 4.2 Å can be observed in all phases, representing the π–π stacking distance between adjacent molecules. The phase behavior exhibited by the assembly of **8a** contrasts with previous work from the Würthner laboratory, which observed only one phase transition below the isotropic state. This phase was assigned as 2D liquid crystalline by these authors.[12] The more detailed phase behavior elucidated here demonstrates the utility of our combined DSC and XRD structural analysis methodology.

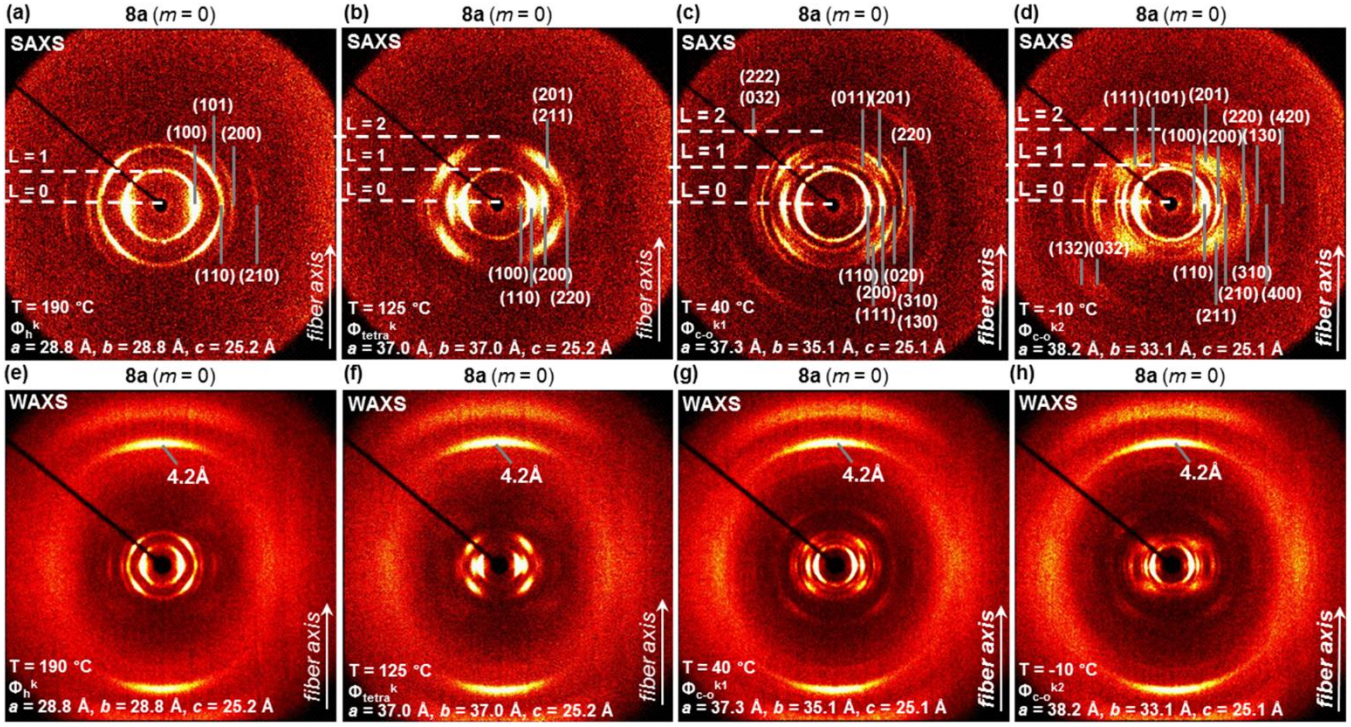

Figure 4. Small angle (a–d) and the corresponding wide angle (e–h) X-ray diffraction patterns obtained from oriented fibers of hydrogenated tetrachlorinated PBI **8a** (m = 0) at indicated temperature and phase. Fiber axis, reflection indexing, temperature, phase, and lattice dimensions are indicated.

Figure 5 shows the SAXS and WAXS patterns and the corresponding reflection indexing and lattice parameters of the periodic arrays assembled from Cl_4PBI compounds **8b** (Figure 5a, e), **8c** (Figure 5b, c, f, g) and **9** (Figure 5d, h). A simple orthorhombic ($\mathbf{\Phi_{s\text{-}o}^{k}}$) unit cell was identified for m = 1 compound **8b** (Figure 5a, e) with an intracolumnar π–π stacking distance of 4.3 Å. The columns are constructed by the stacking of dimers with one molecule per column stratum such that two dimers form a repeating unit along the column direction (c-axis) to give a c-axis length of 17.2 Å (Figure 7d).

Cl_4PBI with m = 2 (**8c**) generates two crystalline periodic arrays. At high temperature (above 75 ºC), a thermodynamically controlled monoclinic ($\mathbf{\Phi_{m}^{k}}$) phase was obtained with an intracolumnar π–π stacking distance of 4.3 Å (Figure 5b, f). At low temperature (below 75 ºC), a kinetically controlled centered orthorhombic ($\mathbf{\Phi_{c\text{-}o}^{k}}$) crystalline phase was observed with an identical intracolumnar stacking distance of 4.3 Å (Figure 5c, g). The sharper reflections in the $\mathbf{\Phi_{c\text{-}o}^{k}}$ phase compared to the $\mathbf{\Phi_{m}^{k}}$ phase indicate that the low temperature $\mathbf{\Phi_{c\text{-}o}^{k}}$ phase, although kinetically controlled, possesses a higher degree of long range order (i.e., longer correlation lengths) than the thermodynamically controlled high temperature $\mathbf{\Phi_{m}^{k}}$ phase.

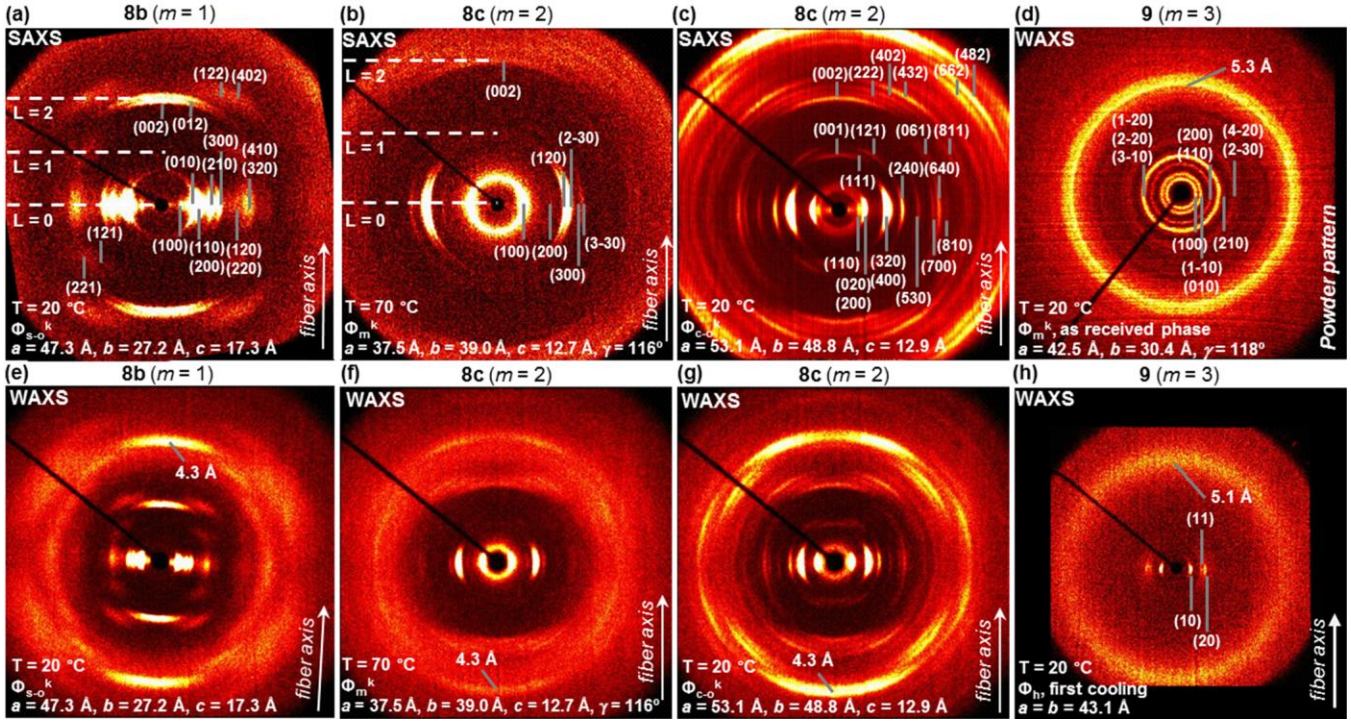

Figure 5. Small angle and the corresponding wide angle X-ray diffraction patterns obtained from oriented fibers of hydrogenated tetrachlorinated PBIs (a, e) **8b** (m = 1) and (b, c, f, g) **8c** (m = 2). Powder (d) and fiber (h) XRD patterns of semifluorinated tetrachlorinated PBI **9** (m = 3) from the as prepared phase and the Φ_h^{io} phase, respectively. Fiber axis, reflection indexing, temperature, phase, and lattice dimensions are indicated.

Semifluorinated compound **9** forms a monoclinic ($\mathbf{\Phi_m^k}$) crystalline phase which is obtained only by precipitation from solution (Figure 5d). The columns are constructed by the stacking of tetramers with two molecules per column stratum (Figure 6d and later discussion), and the column arrangement in this crystalline phase is slightly distorted from perfect hexagonal symmetry. Upon heating to the isotropic state, the $\mathbf{\Phi_m^k}$ crystalline phase cannot be recovered by subsequent cooling and heating treatments. Instead, a 2D ordered hexagonal ($\mathbf{\Phi_h}$) array is obtained. The intracolumnar π–π stacking distance between molecules of **9** in both phases is 5.1–5.3 Å (Figure 5d, h). The detailed structural analysis data obtained from the fiber XRD experiments are summarized in Table 2, and the d-spacings of each reflection observed in the 2D and 3D periodic arrays are listed in Supporting Table ST1.

Table 2. XRD Analysis, Experimental Density and Molecular Weight of Hydrogenated Dendronized Tetrachlorinated PBIs **8a–c** (m = 0, 1, 2) and Semifluorinated Dendronized Cl_4PBIs **9** (m = 3) and **11** (m = 2EO)

Compound	T (°C)	Phase [a]	a, b, c (Å) α, β, γ [b]	D_{col} (Å) [c]	t (Å) [d]	ρ [e] (g/cm^3)	M_{wt} [f]	μ [g]
8a (m = 0)	190	Φ_h^k	28.8, 28.8, 25.2 90°, 90°, 120°	28.8	4.2	1.09	1786.2	1
	125	Φ_{tetra}^k	37.0, 37.0, 25.2 90°, 90°, 90°	26.2	4.2			1
	40	$\Phi_{c\text{-}o}^{k1}$	37.3, 35.1, 25.1 90°, 90°, 90°	25.6	4.2			1
	–10	$\Phi_{c\text{-}o}^{k2}$	38.2, 33.1, 25.1 90°, 90°, 90°	25.3	4.2			1
8b (m = 1)	20	$\Phi_{s\text{-}o}^k$	47.3, 27.2, 17.3 90°, 90°, 90°	27.2	4.3	1.09	1814.3	1
8c (m = 2)	70	Φ_m^k	37.5, 39.0, 12.7 90°, 90°, 116°	37.5	4.2	1.10	1842.3	2
	20	$\Phi_{c\text{-}o}^k$	53.1, 48.8, 12.9 90°, 90°, 90°	36.1	4.3			2
9 (m = 3)	20	$\Phi_m^{k\,h}$	42.5, 30.4, – 90°, 90°, 118°	42.5	5.3	1.70	3705.4	2
	20	Φ_h	43.1, 43.1, – 90°, 90°, 120°	43.1	5.1			2
11 (m = 2EO)	20	Φ_h^{io}**(hc)**	49.5, 49.5, – 90°, 90°, 120°	49.5	5.2	1.73	3853.5	3
	120	Φ_h^{io}**(hc)**	47.5, 47.5, – 90°, 90°, 120°	47.5	5.5			3

[a] Phase notation: Φ_h^k – columnar crystalline hexagonal phase; Φ_{tetra}^k – columnar crystalline tetragonal phase; $\Phi_{c\text{-}o}^k$ – columnar crystalline centered orthorhombic phase; $\Phi_{s\text{-}o}^k$ – columnar crystalline simple orthorhombic phase; Φ_m^k – columnar monoclinic crystalline phase; Φ_h – 2D columnar hexagonal phase with intracolumnar order; Φ_h^{io}**(hc)** – 2D honeycomb-like hexagonal phase with intracolumnar order; [b] Lattice parameters determined from fiber and powder X-ray diffractions. [c] Column diameter calculated using: $D_{col} = a$ for Φ_h, Φ_h^{io}**(hc)**, Φ_h^k and Φ_m^k, and $D_{col} = a$ / [2cos(tan^{-1}(b/a))] for $\Phi_{c\text{-}o}^k$. [d] Stratum thickness calculated from the meridional pattern. [e] Experimental density measured at 20 °C. [f] Molecular weight of the compound. [g] Average number of dendrimers forming the supramolecular column stratum, calculated using: $\mu = N_A \rho A t$ / $2M_{wt}$, where A is the unit cell area of the ab-plane, and t is the average strata thickness calculated from the meridional pattern. [h] Phase observed only in as prepared sample during first heating.

Figure 6 shows and compares the simplified supramolecular columnar structures formed by tetrachlorinated PBIs **8a–c** and **9** and their non-chlorinated analogs. Figure 7 shows the detailed molecular and supramolecular columnar models of the Cl_4PBI derivatives. In the models in Figure 6, the pink spheres indicate the chlorine atoms. The PBI cores (green rectangle) of the Cl_4PBI compounds are distorted because of the steric hindrance and electronic repulsion between adjacent chlorine atoms at the bay position (Figure 7a). This distortion is usually in the range 35°–37º for Cl_4PBIs and shows little dependence on the identity of the groups attached to the imide positions of the Cl_4PBI core.[7,13] This contrasts the non-chlorinated functionalized PBI cores which are planar and typically exhibit a π–π stacking distance of 3.34–3.55 Å in the solid state.[29]

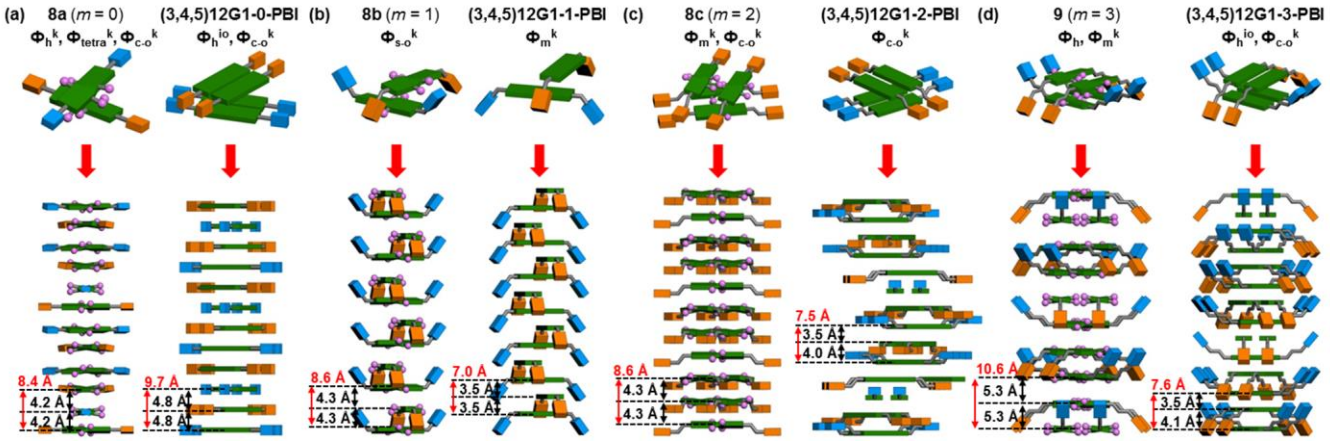

Figure 6. Schematic illustration of the structure of the supramolecular columns self-assembled from (a) tetrachlorinated **8a** (*m* = 0) and non-chlorinated (3,4,5)12G1-0-PBI, (b) tetrachlorinated **8b** (*m* = 1) and non-chlorinated (3,4,5)12G1-1-PBI, (c) tetrachlorinated **8c** (*m* = 2) and non-chlorinated (3,4,5)12G1-2-PBI and (d) semifluorinated tetrachlorinated **9** (*m* = 3) and hydrogenated non-chlorinated PBI (3,4,5)12G1-3-PBI.

The supramolecular columns self-assembled from Cl_4PBI *m* = 0 compound **8a** are constructed from dimers (Figure 7b) while those self-assembled from the non-chlorinated *m* = 0 compound are constructed from tetramers (Figure 6a). The spacing between dimers in both crystal phases formed by **8a** have a uniform intra- and inter-dimer stacking distance of 4.2 Å (Figure 7c). Three dimers form a repeat unit along the column direction (*c*-axis) to generate a *c*-axis length of 25.2 Å (Figure 7d). The relative rotation between neighboring dimers is around 60º. In the non-chlorinated *m* = 0 compound, the columns are formed of tetramers with an inter- and intra-tetramer distance of 4.8 Å. This larger spacing is most likely due to the out-of-plane rotation of the aromatic rings attached to the PBI core in the non-chlorinated system, leading to greater steric hindrance between column strata and thus to a larger π–π stacking distance.[9] The lack of significant out-of-plane rotation of the aromatic ring with respect to the Cl_4PBI core in **8a**, most likely due to the reduced planarity of the Cl_4PBI core, eliminates the steric hindrance observed in the non-chlorinated system and thus permits closer contact between adjacent column strata in the supramolecular columns formed by **8a**. The relative rotation between neighboring tetramers is 90º, leading to a *c*-axis length of 19.3 Å.

The supramolecular columns of both tetrachlorinated and non-chlorinated compounds with *m* = 1 are constructed by dimers with similar intra- and inter-column arrangements. However, whereas neighboring molecules in the columns of the non-chlorinated compound face the same direction, those

in the columns of Cl_4PBI compound **8b** have alternate orientations (Figure 6b). The inter- and intra-dimer distance in **8b** are both 4.3 Å (Figure 7c,d), which is slightly larger than that found in the non-chlorinated analog (3.5 Å). The difference in molecular stacking distance is most likely attributable to the twisted Cl_4PBI core, and gives a larger *c*-axis length in **8b** of 17.2 Å (Figure 7d). The relative rotation between neighboring dimers is 180º so that two dimers form a repeat unit along the *c*-axis.

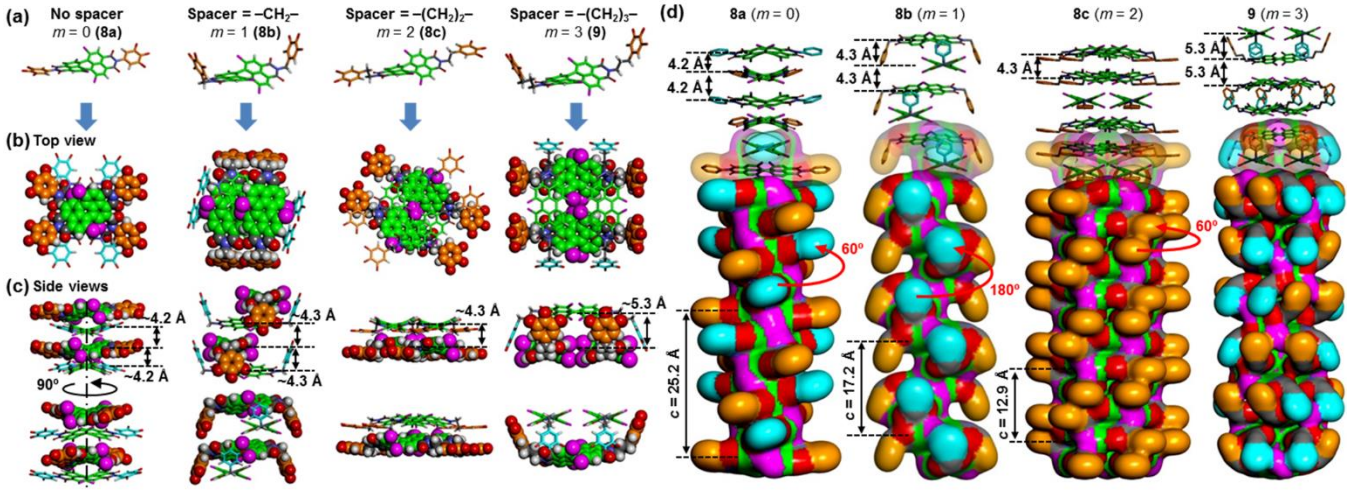

Figure 7. The influence of spacer length on the architecture of supramolecular columns self-assembled from hydrogenated dendronized PBIs **8a–c** (*m* = 0, 1, 2) and semifluorinated dendronized PBI **9** (*m* = 3). (a) Molecular model of the aromatic core region. (b) Top and (c) side views of the supramolecular structures determined by XRD analysis and simulation. (d) Molecular models of the supramolecular columns self-assembled from **8a–c** and **9**. The *c*-axis length and helical rotation parameters are indicated. Color code: O atoms, red; H atoms, white; N atoms, blue; Cl atoms, pink; C atoms of the PBI, green; C atoms of the dendron phenyl group, orange and light blue; all other C atoms, gray. Alkyl chains omitted for clarity.

Although both tetrachlorinated and non-chlorinated compounds with *m* = 2 generate 3D columnar crystalline orthorhombic periodic arrays ($\mathbf{\Phi_{c\text{-}o}^k}$ and $\mathbf{\Phi_{s\text{-}o}^k}$, respectively), their supramolecular columnar structures are quite different. In the non-chlorinated compound, the columns are constructed by stacking of tetramers of molecules with alternating orientation and with non-uniform inter- and intra-tetramer distance (3.5 and 4.0 Å, respectively), and possess an off-center helical rotation (Figure 6c). In Cl_4PBI **8c**, although columns still have two molecules per column as in the non-chlorinated counterpart, the molecule pairs in each stratum do not form tetramers and the stacking distance is uniform (4.3 Å) between adjacent strata. The rotation between adjacent strata is about 60º (Figure 7d). The observations by DSC that the $\mathbf{\Phi_{c\text{-}o}^k}$ phase of **8c** can be developed much more easily than the $\mathbf{\Phi_{s\text{-}o}^k}$ phase of the non-

chlorinated analog and is stable over a much wider temperature range implies that the packing in **8c** leads to more favorable intercolumnar correlations.

Structural Analysis of Cl_4PBIs Dendronized with Semifluorinated Dendrons by SAXS and WAXS. The semifluorinated Cl_4PBI *m* = 3 compound (**9**) does not generate a crystalline phase after its first heating to the isotropic state, most likely due to the increased conformational freedom of the elongated spacer and the stiffness of the semifluorinated alkyl chains at low temperatures. The supramolecular columns in both **9** and a non-chlorinated *m* = 3 compound with hydrogenated dendrons, (3,4,5)12G1-3-PBI, are constructed by the stacking of tetramers (Figure 6d). As in the *m* = 2 systems, the tetrachlorinated *m* = 3 compound (**9**) exhibits a larger, uniform inter- and intra-tetramer stacking distance (5.3 Å) whereas the non-chlorinated compound has smaller, non-uniform inter- and intra-tetramer distances (3.5 and 4.1 Å, respectively). In summary, the chlorination of the PBI core results in a twist of the PBI motif, leading to a larger π–π stacking distance in the bulk state than is typical of non-chlorinated PBIs, and a decrease in T_i of over 100 ºC for **8a** (*m* = 0) and **8b** (*m* = 1) and 25 ºC for **8c** (*m* = 2).

Fiber XRD patterns of **11** (*m* = 2EO) at low temperature and high temperature are shown in Figure 8a and Figure 8c, respectively, and their corresponding reconstructed 2D electron density maps are also provided (Figure 8b, d). Electron density maps were reconstructed from XRD data using a method consistent with previous studies (see Supporting Information and worked example in ref. 27).[27] The molecular conformation in the lattice and a schematic illustration of its hexagonal array are shown in Figure 8e. This compound forms an uncommon honeycomb-like 2D hexagonal array with three molecules in one unit cell. We speculate that the formation of the honeycomb-like structure is a consequence of the extremely flexible ethylene glycol linker between the Cl_4PBI core and the semifluorinated dendrons. The flexibility of this linker permits aggregation of the semifluorinated alkyl chains in the center of the supramolecular columns while the PBI cores are located at the periphery of the columns (Figure 8e). In fact, this honeycomb-like structure bears a lot of similarities to the honeycomb-like liquid crystalline phases exhibited by T-, X-, and anchor-shaped molecules. In those

phases, the rigid aromatic cores of the constituent molecules form the walls of polygonal-shaped columns whose interiors are occupied by flexible side groups.[30,31]

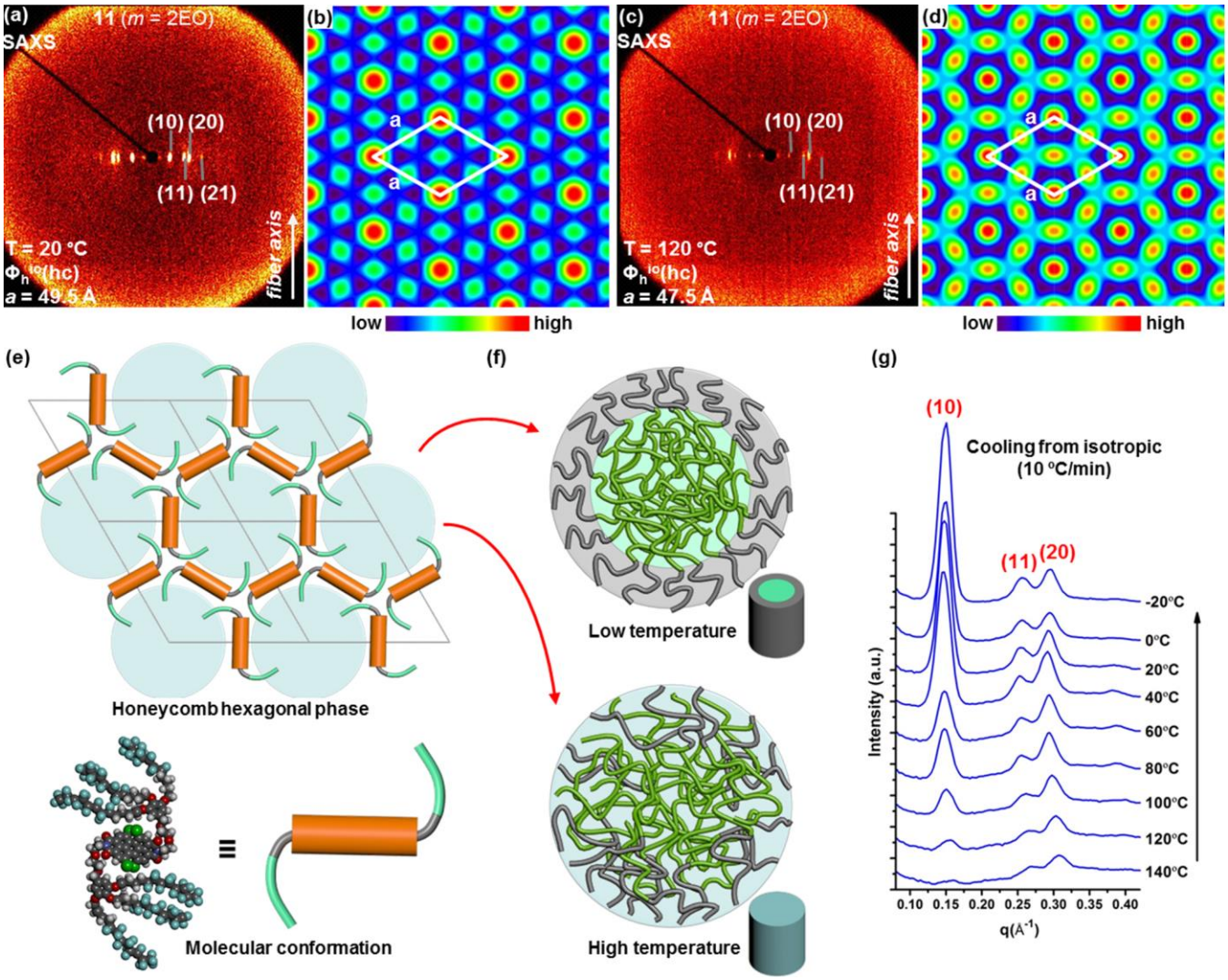

Figure 8. XRD patterns of semifluorinated dendronized PBI **11** (*m* = 2EO) in the 2D honeycomb-like hexagonal phase **(Φ_h^{io}(hc))** collected from an oriented fiber at (a) 20 ºC and (c) 120 ºC. (b, d) The corresponding reconstructed electron density maps. (e) Schematic illustration of the honeycomb-like hexagonal array. (f) Top views of the aggregation of alkyl side chains at low and high temperatures. Gray chains denote –CH_2– units and green chains denote –CF_2– units. (g) Temperature dependent 1D plots of the XRD patterns collected at the indicated temperatures during cooling from the isotropic state.

At low temperatures, the –CF_2– units and –CH_2– units on the alkyl chains are well phase-separated (Figure 8f, top), and therefore the center of columns shows very high electron density (Figure 8b). At high temperatures, this phase separation between –CF_2– and –CH_2– units is less evident due to larger thermal fluctuations (Figure 8f, bottom), and the consequent mixing of the two types of unit leads to a smaller column diameter and a decrease in electron density at the center of the columns (Figure 8d). Furthermore, the relative difference in electron density between the PBI core-based periphery and the

alkyl chain-based column interior becomes smaller. This decrease in the degree of segregation was not detectable by DSC. Indeed, the change in alkyl chain phase segregation is a continuous process, as evidenced by temperature-dependent XRD experiments, which show a continuous change in the relative intensities of the relevant observed reflections (Figure 8g).

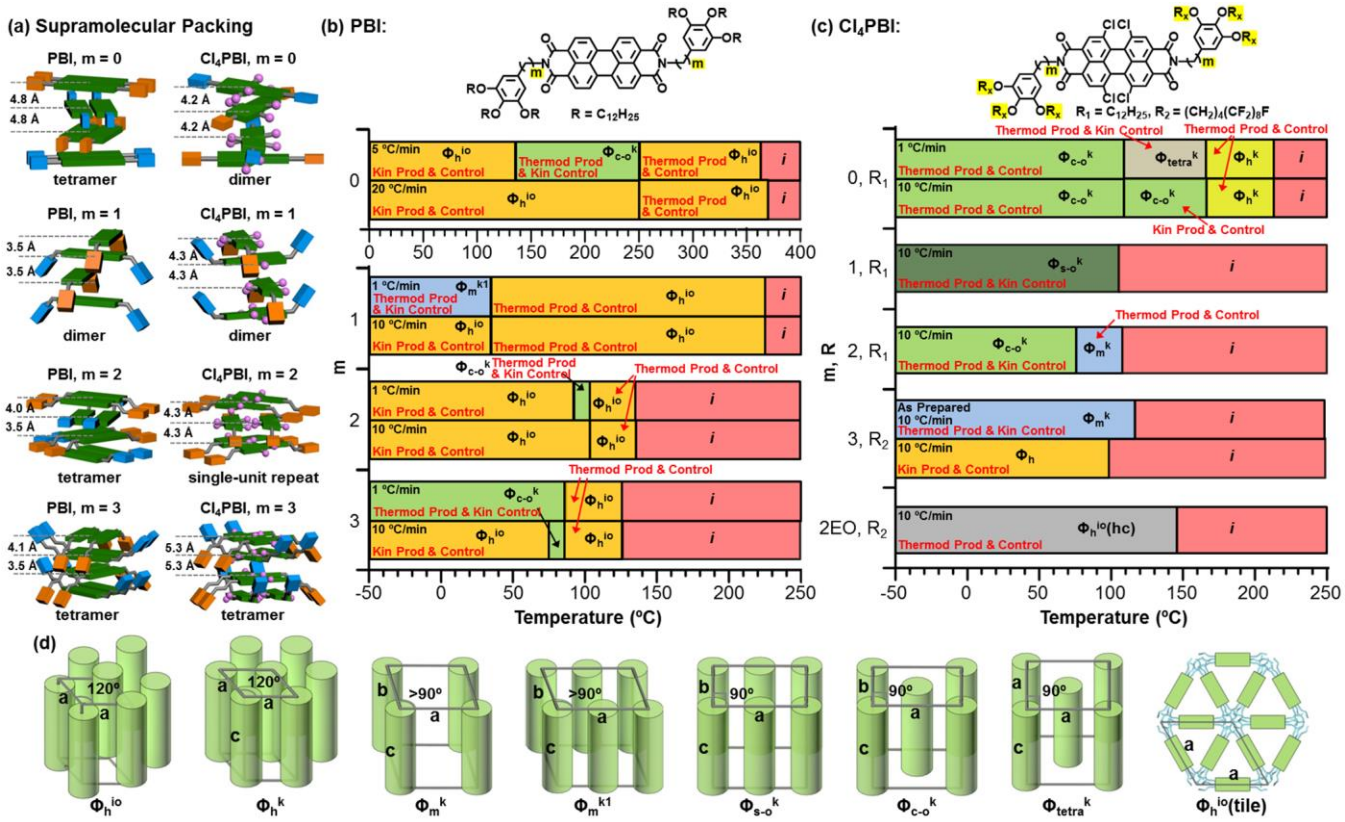

Figure 9. (a) Comparison of the supramolecular packing of dendronized non-chlorinated PBIs and dendronized Cl_4PBIs. (b,c) Diagram of the periodic arrays as a function of *m,* R, and temperature for (b) dendronized non-chlorinated PBIs and (c) dendronized Cl_4PBIs. Data obtained from DSC and XRD analysis at indicated heating rate. (d) Schematic illustration of the arrangement of supramolecular columns in 2D and 3D lattices self-assembled from dendronized non-chlorinated and Cl_4PBIs. Phase notation: $\mathbf{\Phi_h^k}$ – columnar hexagonal crystalline phase; $\mathbf{\Phi_h^{io}}$ – 2D columnar hexagonal phase with intracolumnar order; $\mathbf{\Phi_h}$ – 2D columnar hexagonal phase; $\mathbf{\Phi_{c\text{-}o}^k}$ – columnar centered orthorhombic crystalline phase; $\mathbf{\Phi_{s\text{-}o}^k}$ – columnar simple orthorhombic crystalline phase; $\mathbf{\Phi_m^k}$, $\mathbf{\Phi_m^{k1}}$ – columnar monoclinic crystalline phase; $\mathbf{\Phi_{tetra}^k}$ – columnar tetragonal crystalline phase; $\mathbf{\Phi_h^{io}(hc)}$ – honeycomb-like 2D hexagonal phase; ***iso.*** – isotropic state.

A Comparative Analysis of the Complex Helical Assemblies of Dendronized PBI and Cl_4PBI. Figure 9 depicts the molecular structure, supramolecular columnar structure, phase diagram and the columnar periodic arrays determined by the combination of DSC and XRD for both PBIs and Cl_4PBIs with different spacer length (*m*) and hydrogenated or semifluorinated dendrons. Cl_4PBI compounds **8a–c**, **9** and **11** all exhibit lower T_i values than the corresponding non-chlorinated compounds (Figure 9b).

For m = 0 compound **8a**, the lowering of T_i by tetrachlorination of the PBI core enabled, for the first time, XRD analysis of its phases across the entire temperature range of its non-isotropic behavior. For Cl_4PBI compounds **8b**, **8c** and **9**, T_i lies within a narrow range of temperature (98–110 °C). Compound **11** with m = 2EO has a higher T_i value of 145 °C.

The molecular arrangements within the supramolecular columns formed by **8a–c** and **9** are remarkably similar to the molecular arrangements exhibited by their non-chlorinated PBI counterparts (Figure 9a). In compounds with m = 1, 2 and 3 (**8b**, **8c** and **9**, respectively), the composition of strata within the supramolecular is invariant with respect to tetrachlorination of the PBI core, that is, there is one molecule per stratum in both non-chlorinated and tetrachlorinated m = 1 compounds and two molecules per stratum in m = 2 and 3 compounds. Only in the m = 0 compounds does the number of molecules per column stratum differ.

The major difference between the structure of the columns self-assembled from tetrachlorinated and non-chlorinated PBI derivatives is the π–π stacking between column strata. In contrast to the non-chlorinated m = 2 and 3 compounds, which exhibit different inter- and intra-tetramer stacking distances, the distance between column strata in **8a–c** and **9** is uniform throughout the column. Furthermore, the stacking distance is almost constant for compounds **8a–c** (4.2–4.3 Å), which contrasts with the differing stacking distances exhibited by non-chlorinated m = 0, 1 and 2 compounds (3.5–4.8 Å). In supramolecular columns formed from **8b**, **8c** and **9**, the π–π stacking distance is larger than in columns formed from the corresponding non-chlorinated PBIs, perhaps as a result of the twisting of the PBI core caused by tetrachlorination.[7,13] However, the tetrachlorinated m = 0 compound (**8a**) exhibits a significantly lower π–π stacking distance than the non-chlorinated compound (4.2 Å versus 4.8 Å). The steric hindrance between column strata in the non-chlorinated system, caused by out-of-plane rotation of the aromatic rings attached to the PBI core, is not present in the tetrachlorinated system, permitting closer contact between adjacent strata and thus a smaller π–π stacking distance.

Despite the similarities between the structures formed from Cl_4PBI and PBI derivatives, tetrachlorinated compounds **8a–c** form supramolecular structures with higher order than those formed by

non-chlorinated analogs (Figure 9b, c). Indeed, compounds **8a–c** exhibit only crystalline phases below T_i, in sharp contrast to the Φ_h^{io} phase exhibited most commonly by the non-chlorinated compounds.

Our previous work with non-chlorinated dendronized PBI derivatives demonstrated, for the first time, the thermodynamically controlled formation of 2D and 3D periodic arrays. The tetrachlorinated compounds **8a–c** described in this report demonstrate the thermodynamically controlled formation of exclusively 3D periodic arrays. Furthermore, these compounds provide a new route to stable 3D crystalline phases via thermodynamic control at lower temperatures, thus providing crystalline order in an accessible range of temperature potentially of interest for technological applications.

Solid State NMR Studies on Dendronized Cl_4PBI with *m* = 0, 8a. The induction of higher order in the supramolecular assemblies of the less well ordered Cl_4PBI molecular building block is particularly intriguing. Solid state NMR can probe the packing of the building blocks in supramolecular structures on the molecular level[32] and can therefore verify the structures derived from XRD. In most cases (Figure 9a), the PBI molecules form tetramers constructed from dimers with two molecules packed side by side, and adjacent dimers rotated by approximately 90°. This packing leads to pronounced shifts of several ppm (from ~6 ppm to ~9.5 ppm) in the ^{1}H NMR signals of the PBI aromatic sites for compounds with *m* = 0 to 4 (see Figure 22 in ref. 7).[9] In contrast, *m* = 0 Cl_4PBI compound **8a** forms dimers of two Cl_4PBI molecules perpendicular to each other. These dimers pack into columns in which neighboring dimers are rotated by about 60°. For such packing, no shifts for the aromatic protons of the Cl_4PBI core are expected as deduced from quantum chemical calculations.[33] Moreover, the core protons of **8a**, which have intramolecular distances as large as 7 Å, exhibit intradimer distances of 4.2–4.3 Å only.

Such a structure can be conveniently probed by ^{1}H–^{1}H Double Quantum (DQ) NMR, where the core protons will give rise to strong diagonal peaks.[34,35] This is indeed observed (Figure 10; $1t_r$, where t_r is a rotor time period). This well resolved spectrum differs remarkably from that of the non-chlorinated *m* = 0 PBI counterpart in which the spectral features are broad and unresolved (Figure 10b). Even the proton signals of the Cl_4PBI core at 7.6 ppm are resolved from the signals of the proton in the outer

phenyl rings at 7.2 ppm. Thus, the different packing leads to markedly different ^{1}H–^{1}H DQ NMR spectra and can, therefore, be easily distinguished.

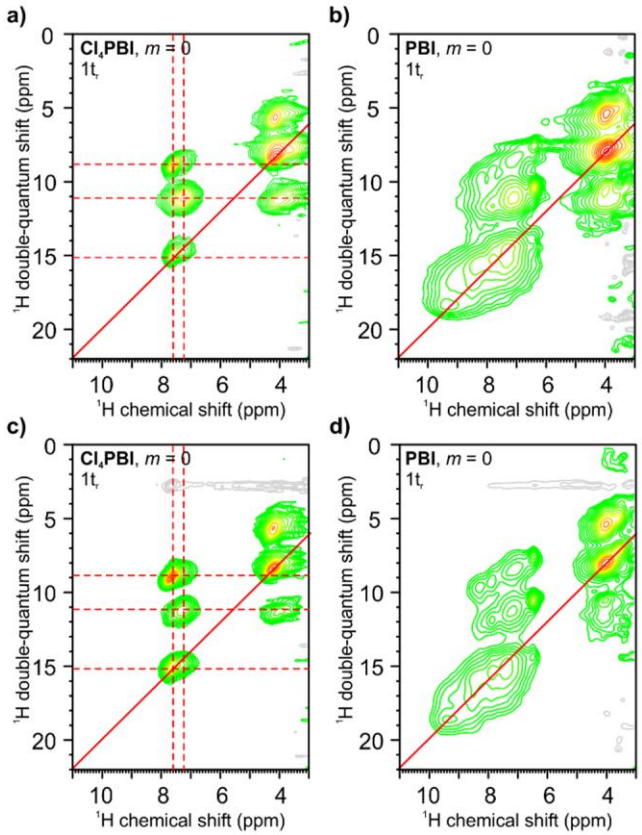

Figure 10. ^{1}H–^{1}H Double Quantum (DQ) NMR correlation spectra[35] recorded at 30 kHz MAS and 850 MHz ^{1}H Larmor frequency. a) $1t_r$ and c) $2t_r$ Back-to-Back (BaBa) DQ excitation for **8a**. b) $1t_r$ and d) $2t_r$ BABA DQ excitation for the non-chlorinated analog, (3,4,5)12G1-0-PBI. The signals of the PBI core and the phenyl rings of the dendron are marked by red dotted lines.

The proton signals of the Cl_4PBI core at 7.6 ppm show a strong diagonal peak due to the proximity of the chemically equivalent protons of the adjacent molecule within the dimer. The proton signals from the phenyl ring of the dendron at 7.2 ppm show a strong correlation to the O–CH_2 sites at 4.15 ppm, which may originate from the intramolecular proximity of the outer phenyl rings and the O-CH_2 sites of the outer alkyl chains at 1.3–1.4 ppm. The aliphatic sites of these alkyl chains in turn show a stronger correlation with the protons of the Cl_4PBI core at 7.6 ppm. Remarkably, the correlation signals of the protons at the core increase in intensity with a longer excitation time ($2t_r$ *vs* $1t_r$, Figure 10), indicating intermolecular proximity, while the local correlations from the outer phenyl ring decrease in intensity, due to local rotational fluctuations interfering with the build-up of DQ coherence.

These findings support the proposed structural model in which the dimerized Cl_4PBI molecules lead to intermolecular dipolar-coupled ^{1}H–^{1}H pairs of initially isolated protons at the Cl_4PBI cores.

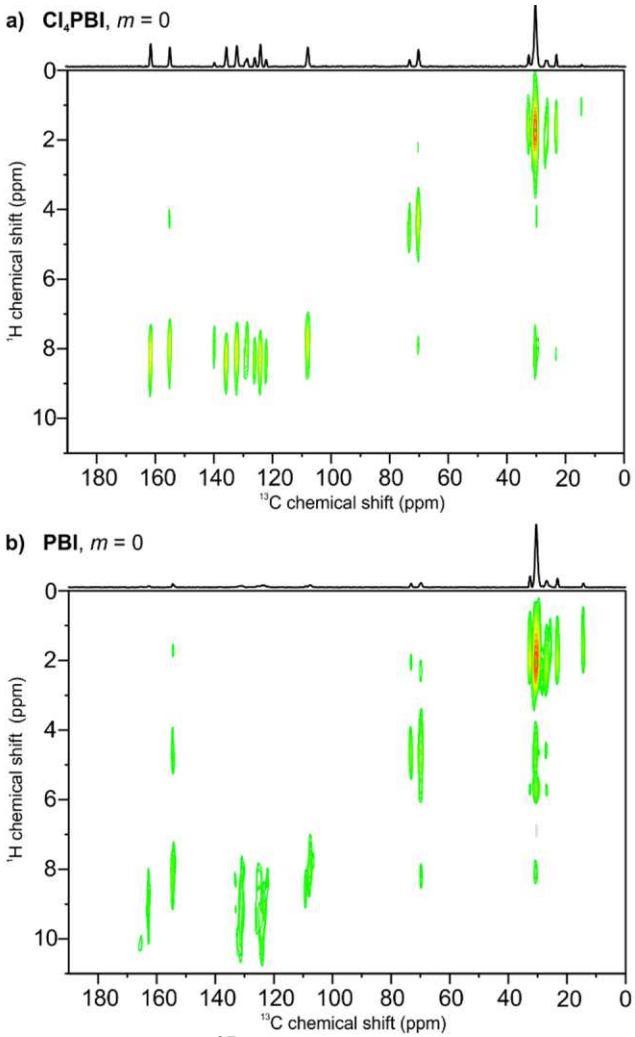

Figure 11. ^{13}C{^{1}H} LG-HETCOR spectra[37] of a) compound **8a** and b) its non-chlorinated analog, (3,4,5)12G1-0-PBI recorded at 700.23 MHz ^{1}H Larmor frequency, 18 KHz MAS and 3 ms CP contact time.

Similar results are deduced from ^{1}H–^{13}C heteronuclear correlation spectra,[36] shown in Figure 11. ^{13}C{^{1}H} Lee-Goldburg-heteronuclear correlation (LG-HETCOR) spectra[37] of **8a** and its non-chlorinated analog confirm the findings of the 2D ^{1}H–^{1}H DQ spectra. Not only is the ^{1}H MAS spectrum of **8a** well resolved, but the regular packing of the chlorinated PBI cores also leads to sharp and well resolved ^{13}C signals, as can be seen from the narrow correlation signals. In fact, the ^{13}C projection of the LG-HETCOR spectrum shows intense signals from the Cl_4PBI core, indicating that the packing of the Cl_4PBI molecules does not lower the local symmetry of the molecular structure (Figure 11a). In contrast, signals of the PBI core are hardly observed in the projection of the LG-HETCOR spectrum of the non-

chlorinated PBI due to the broadening of the signals resulting from the presence of numerous different packing positions for each ^{13}C site of the PBI core (Figure 11b).

Thus, solid state ^{1}H and ^{13}C NMR confirm the structure of the $m = 0$ compound **8a**.

Conclusions

A comparative structural study of the assemblies generated from dendronized Cl_4PBI and PBI derivatives provided an unexpected series of results. Cl_4PBI molecules appended with fully hydrogenated dendrons exhibited exclusively 3D crystalline phases. These 3D phases in the $m = 0$ and $m = 2$ compounds were obtained via thermodynamically controlled self-organization. This observation contrasts with the 2D periodic arrays and kinetically controlled 3D phases exhibited by non-chlorinated PBI analogs, and is unexpected due to the less ordered twisted conformation adopted by the Cl_4PBI core rather than the more ordered planar conformation favored by non-chlorinated PBI. Furthermore, the Cl_4PBI with $m = 0$ exhibits closer π–π stacking (by XRD) and more regular molecular packing (by NMR) than its non-chlorinated analog. Hence the presence of disorder at the molecular level induces higher order at the supramolecular level. In contrast, semifluorination and tetrachlorination in an $m = 3$ compound eliminates the orthorhombic crystal observed in the non-chlorinated compound. Consequently the Cl_4PBI with $m = 3$ exhibits only a 2D columnar hexagonal array, as would be expected from the reduced flexibility of the semifluorinated chain compared to a perhydrogenated chain. However, the addition of an ethylene glycol linker promotes crystallization in the semifluorinated Cl_4PBI, generating an unusual honeycomb structure with intracolumar order and temperature-dependent phase segregation. Therefore, the tetrachlorinated PBIs reported here, and the thermally accessible supramolecular assemblies organized therefrom, represent a new series of structures of interest for organic electronics, photovoltaics and other electronic applications. The correlation between molecular disorder and supramolecular order elaborated here also provides a new general strategy for the generation of other highly ordered supramolecular materials.

Supporting Information

Experimental procedures with complete spectral and structural analysis. This material is available free of charge via the Internet at http://pubs.acs.org.

AUTHOR INFORMATION

Corresponding Author

percec@sas.upenn.edu

Notes

The authors declare no competing financial interests.

ACKNOWLEDGMENTS

Financial support by the National Science Foundation (DMR-1066116, DMR-1120901 and OISE-1243313), the Humboldt Foundation and the P. Roy Vagelos Chair at Penn (all to VP) is gratefully acknowledged. GU and XZ acknowledge support from the joint NSF-EPSRC PIRE project "RENEW" (EPSRC grant EP-K034308). We thank Dr. Shaodong Zhang for his assistance in obtaining ^{1}H NMR spectra.

REFERENCES

(1) Würthner, F. *Chem. Commun.* **2004**, 1564–1579.

(2) Zhang, X.; Rehm, S.; Safont-Sempere, M. M.; Würthner, F. *Nat. Chem.* **2009**, *1*, 623–629.

(3) Rybtchinski, B.; Sinks, L. E.; Wasielewski, M. R. *J. Am. Chem. Soc.* **2004**, *126*, 12268–12269.

(4) Eakins, G. L.; Gallaher, J. K.; Keyzers, R. A.; Falber, A.; Webb, J. E. A.; Laos, A.; Tidhar, Y.; Weissman, H.; Rybtchinski, B.; Thordarson, P.; Hodgkiss, J. M. *J. Phys. Chem. B* **2014**, *118*, 8642–8651.

(5) Huang, C.; Barlow, S.; Marder, S. R. *J. Org. Chem.* **2011**, *76*, 2386–2407.

(6) Zhan, X.; Facchetti, A.; Barlow, S.; Marks, T. J.; Ratner, M. A.; Wasielewski, M. R.; Marder, S. R. *Adv. Mater.* **2011**, *23*, 268–284.

(7) Chen, Z.; Baumeister, U.; Tschierske, C.; Würthner, F. *Chem. Eur. J.* **2007**, *13*, 450–465.

(8) Schmidt, R.; Ling, M. M.; Oh, J. H.; Winkler, M.; Könemann, M.; Bao, Z.; Würthner, F. *Adv. Mater.* **2007**, *19*, 3692–3695.

(9) Percec, V.; Peterca, M.; Tadjiev, T.; Zeng, X.; Ungar, G.; Leowanawat, P.; Aqad, E.; Imam, M. R.; Rosen, B. M.; Akbey, U.; Graf, R.; Sekharan, S.; Sebastiani, D.; Spiess, H. W.; Heiney, P. A.; Hudson, S. D. *J. Am. Chem. Soc.* **2011**, *133*, 12197–12219.

(10) Percec, V.; Hudson, S. D.; Peterca, M.; Leowanawat, P.; Aqad, E.; Graf, R.; Spiess, H. W.; Zeng, X.; Ungar, G.; Heiney, P. A. *J. Am. Chem. Soc.* **2011**, *133*, 18479–18494.

(11) Percec, V.; Sun, H.-J.; Leowanawat, P.; Peterca, M.; Graf, R.; Spiess, H. W.; Zeng, X.; Ungar, G.; Heiney, P. A. *J. Am. Chem. Soc.* **2013**, *135*, 4129–4148.

(12) Debije, M. G.; Chen, Z.; Piris, J.; Neder, R. B.; Watson, M. M.; Müllen, K.; Würthner, F. *J. Mater. Chem.* **2005**, *15*, 1270–1276.

(13) Chen, Z.; Debije, M. G.; Debaerdemaeker, T.; Osswald, P.; Würthner, F. *ChemPhysChem* **2004**, *5*, 137–140.

(14) Schmidt, R.; Oh, J. H.; Sun, Y.-S.; Deppisch, M.; Krause, A.-M.; Radacki, K.; Braunschweig, H.; Könemann, M.; Erk, P.; Bao, Z.; Würthner, F. *J. Am. Chem. Soc.* **2009**, *131*, 6215–6228.

(15) Percec, V.; Peterca, M.; Sienkowska, M. J.; Ilies, M. A.; Aqad, E.; Smidrkal, J.; Heiney, P. A. *J. Am. Chem. Soc.* **2006**, *128*, 3324–3334.

(16) Johansson, G.; Percec, V.; Ungar, G.; Zhou, J. P. *Macromolecules* **1996**, *29*, 646–660.

(17) Sadrai, M.; Hadel, L.; Sauers, R. R.; Husain, S.; Krogh-Jespersen, K.; Westbrook, J. D.; Bird, G. R. *J. Phys. Chem.* **1992**, *96*, 7988–7996.

(18) Johansson, G.; Percec, V.; Ungar, G.; Smith, K. *Chem. Mater.* **1997**, *9*, 164–175.

(19) Percec, V.; Schlueter, D.; Kwon, Y. K.; Blackwell, J.; Moeller, M.; Slangen, P. J. *Macromolecules* **1995**, *28*, 8807–8818.

(20) Dukeson, D. R.; Ungar, G.; Balagurusamy, V. S. K.; Percec, V.; Johansson, G. A.; Glodde, M. *J. Am. Chem. Soc.* **2003**, *125*, 15974–15980.

(21) Percec, V.; Glodde, M.; Johansson, G.; Balagurusamy, V. S. K.; Heiney, P. A. *Angew. Chem. Int. Ed.* **2003**, *42*, 4338–4342.

(22) Percec, V.; Johansson, G.; Ungar, G.; Zhou, J. *J. Am. Chem. Soc.* **1996**, *118*, 9855–9866.

(23) Percec, V.; Glodde, M.; Bera, T. K.; Miura, Y.; Shiyanovskaya, I.; Singer, K. D.; Balagurusamy, V. S. K.; Heiney, P. A.; Schnell, I.; Rapp, A.; Spiess, H.-W.; Hudson, S. D.; Duan, H. *Nature* **2002**, *419*, 384–387.

(24) Percec, V.; Glodde, M.; Peterca, M.; Rapp, A.; Schnell, I.; Spiess, H. W.; Bera, T. K.; Miura, Y.; Balagurusamy, V. S. K.; Aqad, E.; Heiney, P. A. *Chem. Eur. J.* **2006**, *12*, 6298.

(25) Percec, V.; Aqad, E.; Peterca, M.; Imam, M. R.; Glodde, M.; Bera, T. K.; Miura, Y.; Balagurusamy, V. S. K.; Ewbank, P. C.; Würthner, F.; Heiney, P. A. *Chem. Eur. J.* **2007**, *13*, 3330–3345.

(26) Wilson, C. J.; Wilson, D. A.; Feiring, A. E.; Percec, V. *J. Polym. Sci. Part A Polym. Chem.* **2010**, *48*, 2498–2508.

(27) Wu, Y.-C.; Leowanawat, P.; Sun, H.-J.; Partridge, B. E.; Peterca, M.; Graf, R.; Spiess, H. W.; Zeng, X.; Ungar, G.; Hsu, C.-S.; Heiney, P. A; Percec, V. *J. Am. Chem. Soc.* **2015**, *137*, 807–819.

(28) Roche, C.; Sun, H.-J.; Prendergast, M. E.; Leowanawat, P.; Partridge, B. E.; Heiney, P. A; Araoka, F.; Graf, R.; Spiess, H. W.; Zeng, X.; Ungar, G.; Percec, V. *J. Am. Chem. Soc.* **2014**, *136*, 7169–7185.

(29) Klebe, G.; Graser, F.; Hädicke, E.; Berndt, J. *Acta Crystallogr. Sect. B Struct. Sci.* **1989**, *45*, 69–77.

(30) Glettner, B.; Liu, F.; Zeng, X.; Prehm, M.; Baumeister, U.; Ungar, G.; Tschierske, C. *Angew. Chem. Int. Ed.* **2008**, *47*, 6080–6083.

(31) Tschierske, C.; Nürnberger, C.; Ebert, H.; Glettner, B.; Prehm, M.; Liu, F.; Zeng, X.-B.; Ungar, G. *Interface Focus* **2012**, *2*, 669–680.

(32) Hansen, M. R.; Graf, R.; Spiess, H. W. *Acc. Chem. Res.* **2013**, *46*, 1996–2007.

(33) Hansen, M. R.; Graf, R.; Sekharan, S.; Sebastiani, D. *J. Am. Chem. Soc.* **2009**, *131*, 5251–5256.

(34) Brown, S. P.; Spiess, H. W. *Chem. Rev.* **2001**, *101*, 4125–4155.

(35) Feike, M.; Demco, D. E.; Graf, R.; Gottwald, J.; Hafner, S.; Spiess, H. W. *J. Magn. Reson. Ser. A* **1996**, *122*, 214–221.

(36) Schmidt-Rohr, K.; Spiess, H. W. *Multidimensional solid-state NMR and polymers*; Academic Press: New York, 1994.

(37) Van Rossum, B.-J.; Förster, H.; de Groot, H. J. M. *J. Magn. Reson.* **1997**, *124*, 516–519.

TOC Graphic

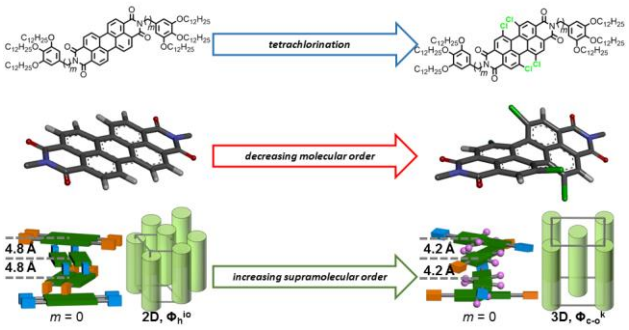
tetrachlorination
decreasing molecular order
increasing supramolecular order
4.8 Å
4.8 Å
m = 0
2D, Φh^io
4.2 Å
4.2 Å
m = 0
3D, Φc-o^k